

1-1-2010

## Solvothermal synthesis of ternary sulfides of $\text{Sb}_2\text{xBi}_x\text{S}_3$ ( $x=0.4,1$ ) with 3D flower-like architectures

Jiquan Sun  
*Jiangsu University China*

Xiaoping Shen  
*Jiangsu University China, xshen@uow.edu.au*

Lijun Guo  
*Jiangsu University*

Guoxiu Wang  
*University of Wollongong, gwang@uow.edu.au*

Jinsoo Park  
*University of Wollongong, jp450@uow.edu.au*

*See next page for additional authors*

Follow this and additional works at: <https://ro.uow.edu.au/engpapers>

 Part of the [Engineering Commons](#)

<https://ro.uow.edu.au/engpapers/4181>

---

### Recommended Citation

Sun, Jiquan; Shen, Xiaoping; Guo, Lijun; Wang, Guoxiu; Park, Jinsoo; and Wang, Kun: Solvothermal synthesis of ternary sulfides of  $\text{Sb}_2\text{xBi}_x\text{S}_3$  ( $x=0.4,1$ ) with 3D flower-like architectures 2010, 364-369. <https://ro.uow.edu.au/engpapers/4181>

---

**Authors**

Jiquan Sun, Xiaoping Shen, Lijun Guo, Guoxiu Wang, Jinsoo Park, and Kun Wang

# Solvothermal Synthesis of Ternary Sulfides of $\text{Sb}_{2-x}\text{Bi}_x\text{S}_3$ ( $x = 0.4, 1$ ) with 3D Flower-Like Architectures

Jiquan Sun · Xiaoping Shen · Lijun Guo ·  
Guoxiu Wang · Jinsoo Park · Kun Wang

Received: 19 May 2009 / Accepted: 31 October 2009 / Published online: 13 November 2009  
© to the authors 2009

**Abstract** Flower-like nanostructures of  $\text{Sb}_{2-x}\text{Bi}_x\text{S}_3$  ( $x = 0.4, 1.0$ ) were successfully prepared using both antimony diethyldithiocarbamate [ $\text{Sb}(\text{DDTC})_3$ ] and bismuth diethyldithiocarbamate [ $\text{Bi}(\text{DDTC})_3$ ] as precursors under solvothermal conditions at 180 °C. The prepared  $\text{Sb}_{2-x}\text{Bi}_x\text{S}_3$  with flower-like 3D architectures were characterized by X-ray diffraction (XRD), scanning electron microscopy (SEM), energy dispersive X-ray spectrometry (EDS), high-resolution transmission electron microscopy (HRTEM), and selected area electron diffraction (SAED). The flower-like architectures, with an average diameter of  $\sim 4 \mu\text{m}$ , were composed of single-crystalline nanorods with orthorhombic structures. The optical absorption properties of the  $\text{Sb}_{2-x}\text{Bi}_x\text{S}_3$  nanostructures were investigated by UV–Visible spectroscopy, and the results indicate that the  $\text{Sb}_{2-x}\text{Bi}_x\text{S}_3$  compounds are semiconducting with direct band gaps of 1.32 and 1.30 eV for  $x = 0.4$  and 1.0, respectively. On the basis of the experimental results, a possible growth mechanism for the flower-like  $\text{Sb}_{2-x}\text{Bi}_x\text{S}_3$  nanostructures is suggested.

**Keywords** Nanostructures · Semiconductor · Ternary sulfide · Solvothermal · Optical properties

## Introduction

Semiconductor nanocrystals have attracted much attention in the past few decades [1, 2]. Among them, binary chalcogenide semiconductors of the  $\text{A}_2\text{E}_3^{\text{VI}}$  type ( $\text{A}=\text{Sb, Bi}$ ;  $\text{E}=\text{S, Se, Te}$ ) have aroused great interest due to their potential and practical applications in thermoelectric and optoelectronic devices. For example, bismuth sulfide ( $\text{Bi}_2\text{S}_3$ ), which crystallizes in the orthorhombic system, is a direct band gap semiconductor with  $E_{\text{g}} = 1.3 \text{ eV}$  and can be applied in photovoltaic converters [3] and thermoelectric cooling technologies based on the Peltier effect [4]. At the same time,  $\text{Bi}_2\text{S}_3$  nanocrystalline films have been found to significantly alter the performance of photochemical cells due to quantum size effects [5]. Moreover, antimony sulfide ( $\text{Sb}_2\text{S}_3$ ), which is isostructural to  $\text{Bi}_2\text{S}_3$ , shows interesting high photosensitivity and high thermoelectric power [6], and its direct band gap of 1.5–2.50 eV covers the visible and near infrared range of the solar spectrum [7–9]. As a result,  $\text{Sb}_2\text{S}_3$  has wide applications in solar energy conversion, thermoelectric cooling technologies, television cameras, microwave devices, switching devices, rechargeable storage cells, and optoelectronics in the infrared (IR) region [10–13].

The band gap of a material determines its applicability as an optoelectronic material; therefore, tailoring of the band gap is very helpful. A usual approach to adjust the band gap is to synthesize materials on the nanoscale to take advantage of the quantum confinement effect. However, due to the low Bohr radius of most materials, the method is often far from effective. As an alternative, the band gap can also be tailored by adjusting the composition of materials. It is well known that in doped compound semiconductors, in contrast to undoped ones, the impurity states play a special role in the electronic energy structures and transition probabilities [14]. For doped nanocrystalline

J. Sun · X. Shen (✉) · L. Guo · K. Wang  
School of Chemistry and Chemical Engineering,  
Jiangsu University, 212003 Zhenjiang, China  
e-mail: xiaopingshen@163.com

G. Wang · J. Park  
School of Mechanical, Materials and Mechatronics Engineering,  
University of Wollongong, Wollongong, NSW 2522, Australia

semiconductor compounds, confinement effects in the energy states also produce unusual physical and optical behavior. Recently, several research groups have reported the effects of the composition on the quantum efficiency of  $\text{Zn}_{1-x}\text{Mn}_x\text{S}$  and  $\text{Cd}_x\text{Zn}_{1-x}\text{S}$  nanoparticles [15–18]. In this paper, for the first time, we report the synthesis and band gap of Bi-doped  $\text{Sb}_2\text{S}_3$  ternary sulfides,  $\text{Sb}_{2-x}\text{Bi}_x\text{S}_3$  ( $x = 0.4, 1.0$ ) with flower-like nanostructures, prepared by a facile solvothermal method.

## Experimental

All the chemical reagents used in our experiments were of analytical grade and were used without further purification. The molecular precursors, antimony and bismuth diethyldithiocarbamate,  $\text{Sb}(\text{DDTC})_3$  and  $\text{Bi}(\text{DDTC})_3$ , were prepared as follows: 0.01 mol of  $\text{SbCl}_3$  [or  $\text{Bi}(\text{NO}_3)_3$ ] and 0.02 mol of  $(\text{C}_2\text{H}_5)_2\text{NCS}_2\text{Na}\cdot 3\text{H}_2\text{O}$  were dissolved in 100 mL of distilled water, respectively. Then, the two solutions were mixed by stirring in a 500-mL beaker. The resulting white precipitates were filtered, washed with distilled water, and dried in air at 60 °C.

In a typical procedure for synthesizing  $\text{Sb}_{2-x}\text{Bi}_x\text{S}_3$ , the molecular precursors of  $\text{Sb}(\text{DDTC})_3$  and  $\text{Bi}(\text{DDTC})_3$  in the appropriate ratios (1 mmol in all) were put into a Teflon-lined stainless steel autoclave (30 mL capacity) to which 20 mL of ethylene glycol was added. The autoclave was sealed and maintained at 180 °C for 12 h; then it was allowed to cool to room temperature naturally. The as-formed black precipitates were separated by centrifugation, washed with ethanol and distilled water several times, and dried at 60 °C for 3 h.

The phase of the as-synthesized products was characterized using X-ray diffraction (XRD, Shimadzu XRD-6000) with  $\text{Cu K}\alpha$  radiation ( $\lambda = 1.5406 \text{ \AA}$ ) at a scanning rate of  $4^\circ \text{ min}^{-1}$ . The X-ray tubes were operated with electric current of 30 mA and voltage of 40 kV. The composition, morphology, and sizes of the products were examined by field emission scanning electron microscopy (FESEM; JSM-7001), energy dispersive X-ray spectroscopy (EDS), and transmission electron microscopy (TEM; JEOL-2100). Samples for TEM were prepared by dropping the products on a carbon-coated copper grid after ultrasonic dispersion in absolute ethanol. The band gap energy of the products was determined from the onset of the absorbance spectra of the samples on a UV–Visible (UV–Vis) spectrophotometer with near IR (NIR) capability (Shimadzu UV-4100).

## Results and Discussion

Figure 1 shows the XRD patterns of the as-synthesized products, and the diffraction peaks of both  $\text{Sb}_{2-x}\text{Bi}_x\text{S}_3$

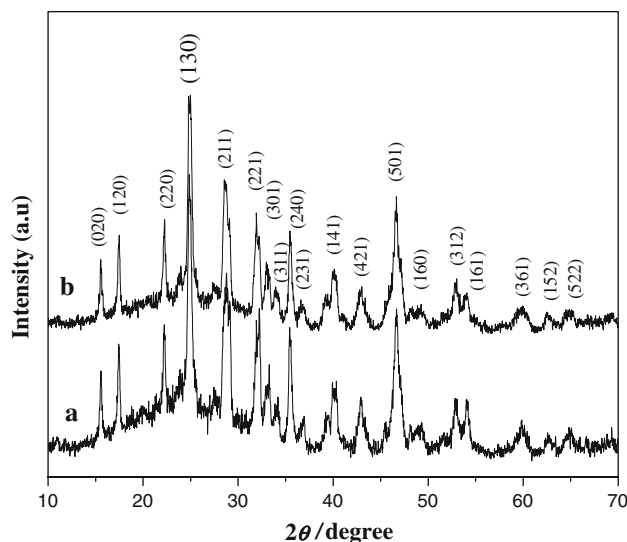


**Fig. 1** XRD patterns of the flower-like  $\text{Sb}_{2-x}\text{Bi}_x\text{S}_3$ : (a)  $x = 0.4$ ; (b)  $x = 1$

samples can be indexed as orthorhombic phase structures with lattice constants of  $a = 11.182 \text{ \AA}$ ,  $b = 11.378 \text{ \AA}$ , and  $c = 3.991 \text{ \AA}$ , and  $a = 11.151 \text{ \AA}$ ,  $b = 11.375 \text{ \AA}$ , and  $c = 4.026 \text{ \AA}$  for  $x = 0.4$  and  $1.0$  ( $\text{Sb}_{1.6}\text{Bi}_{0.4}\text{S}_3$  and  $\text{SbBiS}_3$ ), respectively. The XRD patterns are consistent with the orthorhombic phases  $\text{Sb}_2\text{S}_3$  (JCPDS: 42-1393) and  $\text{Bi}_2\text{S}_3$  (JCPDS: 17-0320). EDS analyses were employed to determine the chemical composition of the products. The EDS spectra (Fig. 2a, b) taken from the nanoflowers in SEM measurements show that both the samples are composed of S, Bi, and Sb elements with molar ratios (Bi:Sb) of about 1:4 and 1:1, respectively. To clarify whether the nanorods were pure  $\text{Sb}_{2-x}\text{Bi}_x\text{S}_3$  or a mixture of  $\text{Bi}_2\text{S}_3$  and  $\text{Sb}_2\text{S}_3$ , EDS from individual nanorods was examined using TEM. As shown in Fig. 2c and d, each of the nanorods contained S, Bi, and Sb elements with a molar ratio similar to the case in SEM. The signals for Cu and C in the EDS spectra came from the carbon-coated copper grid used for TEM measurement. These results confirmed the successful preparation of bismuth and antimony ternary sulfides.

The overall morphology of the  $\text{Sb}_{1.6}\text{Bi}_{0.4}\text{S}_3$  is shown in Fig. 3a, which illustrates that the obtained products consist of a large number of flower-like nanostructures. After careful observation (Fig. 3b), it was found that the flower-like architectures consist of several nanorod bundles that are  $\sim 4 \mu\text{m}$  in length and extend toward many different directions. Furthermore, every nanorod bundle is made up of nanorods with a diameter of  $\sim 80 \text{ nm}$ . The overall morphology of the  $\text{SbBiS}_3$  is shown in Fig. 3c. It can be seen that similar to the  $\text{Sb}_{1.6}\text{Bi}_{0.4}\text{S}_3$ , the  $\text{SbBiS}_3$  products also consist of a large number of flower-like

**Fig. 2** EDS spectra of the  $\text{Sb}_{2-x}\text{Bi}_x\text{S}_3$  nanoflowers and individual nanorods shown in the respective *insets*:

**a, c**  $x = 0.4$ ; **b, d**  $x = 1$

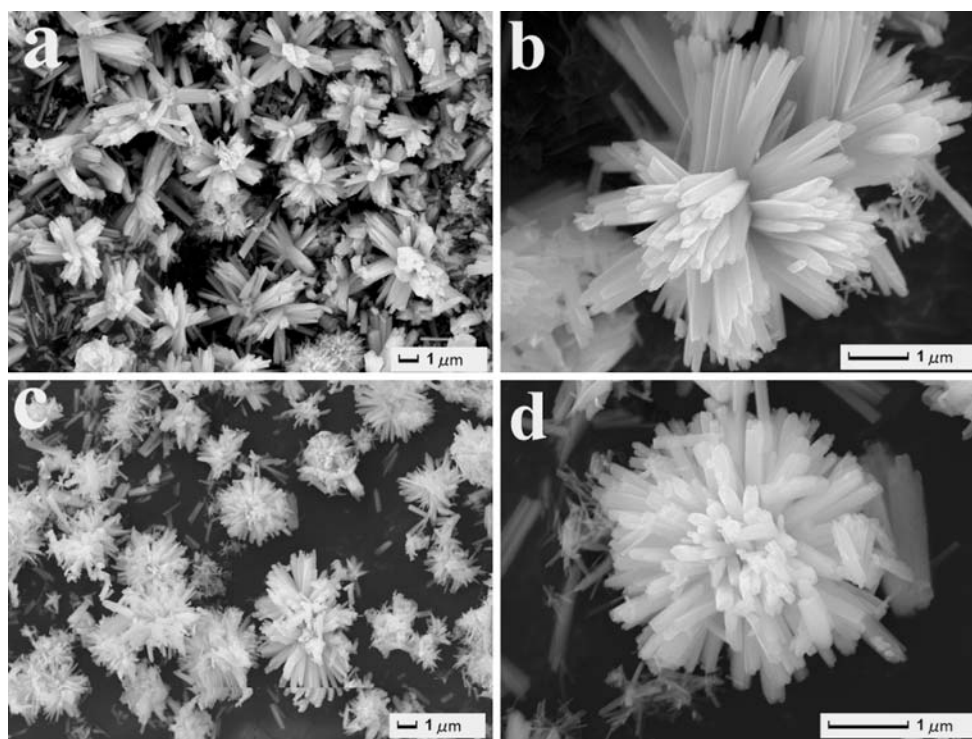
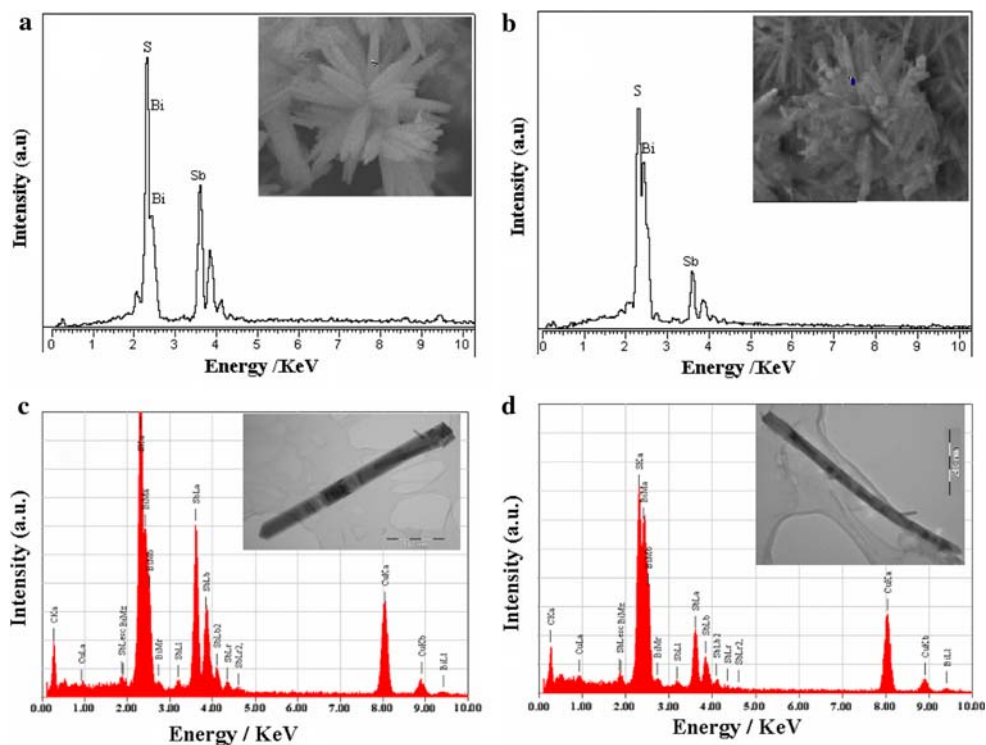


**Fig. 3** FESEM images of the flower-like  $\text{Sb}_{2-x}\text{Bi}_x\text{S}_3$ : **a, b**  $x = 0.4$ ; **c, d**  $x = 1$

nanostructures. However, as shown in Fig. 3d, the flower-like architectures of  $\text{SbBiS}_3$  have a highly regular sphere-like morphology, which is obviously different from that of  $\text{Sb}_{1.6}\text{Bi}_{0.4}\text{S}_3$ . The sphere-like structure with

an average diameter of about  $4 \mu\text{m}$  is composed of large numbers of nanorods, which grow radially from the central core and have a length of  $2 \mu\text{m}$  and a diameter of about  $100 \text{nm}$ .

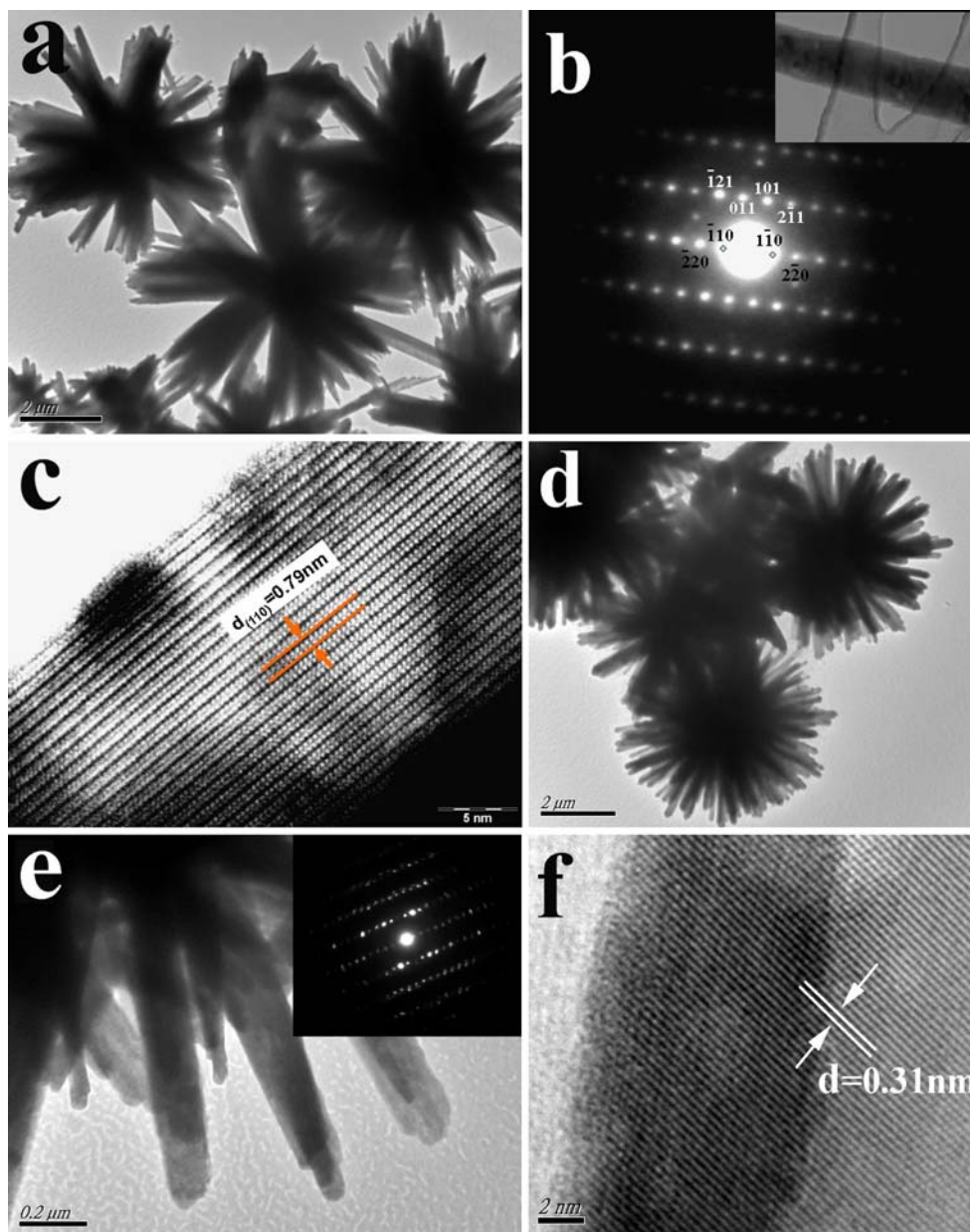


**Fig. 4** TEM, HRTEM, and SAED images of the  $\text{Sb}_{2-x}\text{Bi}_x\text{S}_3$ : **a–c**  $x = 0.4$ ; **d–f**  $x = 1$

A further investigation of the  $\text{Sb}_{2-x}\text{Bi}_x\text{S}_3$  products was made by TEM. Figure 4a shows a typical TEM image of  $\text{Sb}_{1.6}\text{Bi}_{0.4}\text{S}_3$  flower-like architectures, which is consistent with the FESEM observations. After long ultrasonic treatment during the preparation of the TEM specimens, the flower-like structures were substantially unaffected. This suggests that the formation of the flower-like architectures is not due to aggregation. The microstructures of the  $\text{Sb}_{1.6}\text{Bi}_{0.4}\text{S}_3$  nanorods were investigated by high-resolution TEM (HRTEM) and selected area electron diffraction (SAED). The SAED pattern (Fig. 4b) taken from an individual nanorod indicated in the inset shows regular diffraction spots, which can be indexed as a orthorhombic

$\text{Sb}_{1.6}\text{Bi}_{0.4}\text{S}_3$  single crystal recorded from the  $[11-1]$  zone axis and demonstrates that the  $\text{Sb}_{1.6}\text{Bi}_{0.4}\text{S}_3$  nanorod grows along the  $[1-10]$  direction. As shown in Fig. 4c, the HRTEM image of the  $\text{Sb}_{1.6}\text{Bi}_{0.4}\text{S}_3$  nanorod shows clear lattice fringes with a  $d$ -spacing of 0.79 nm, which corresponds to the  $(110)$  lattice distance. Figure 4d shows a TEM image of the  $\text{SbBiS}_3$  sample. It can be seen that the  $\text{SbBiS}_3$  has a perfect sphere-like architecture consisting of nanorods, which is agreement with the FESEM observations. The nanorods extend radially from the central core and have less regular shapes (Fig. 4e). The SAED pattern (inset in Fig. 4e) taken from an individual nanorod shows that the  $\text{SbBiS}_3$  nanorod is single-crystalline. Figure 4f

depicts a HRTEM image of the  $\text{SbBiS}_3$  nanorod. The clear lattice fringes with a  $d$ -spacing of 0.31 nm are consistent with that of the (211) planes of orthorhombic  $\text{SbBiS}_3$ , further confirming that the  $\text{SbBiS}_3$  nanorod is single-crystalline.

In our previous study,  $\text{Bi}(\text{DDTC})_3$  and  $\text{Sb}(\text{DDTC})_3$  have been used as single-source molecular precursors for the syntheses of  $\text{Bi}_2\text{S}_3$  [19] and  $\text{Sb}_2\text{S}_3$  [20] nanomaterials, respectively. Considering the highly similar crystal structures of  $\text{Bi}_2\text{S}_3$  and  $\text{Sb}_2\text{S}_3$ , we herein synthesized ternary sulfides  $\text{Sb}_{2-x}\text{Bi}_x\text{S}_3$  by using both  $\text{Bi}(\text{DDTC})_3$  and  $\text{Sb}(\text{DDTC})_3$  as precursors in a one-pot reaction. Based on the experimental observations, we infer that the formation process of the flower-like  $\text{Sb}_{2-x}\text{Bi}_x\text{S}_3$  nanostructures can be divided into three steps: First, under the solvothermal action, the precursors of  $\text{Bi}(\text{DDTC})_3$  and  $\text{Sb}(\text{DDTC})_3$  were decomposed and produced  $\text{Sb}_{2-x}\text{Bi}_x\text{S}_3$ , which would form  $\text{Sb}_{2-x}\text{Bi}_x\text{S}_3$  crystal nuclei when the degree of supersaturation of the  $\text{Sb}_{2-x}\text{Bi}_x\text{S}_3$  reached a certain critical point. Secondly, these crystal nuclei grew and/or aggregated into a bigger core, which was thermodynamically favorable due to the decrease in the surface energy. Finally, the as-formed cores may serve as the substrates for epitaxial growth of the  $\text{Sb}_{2-x}\text{Bi}_x\text{S}_3$  nanorods. As a result, the flower-like architecture with  $\text{Sb}_{2-x}\text{Bi}_x\text{S}_3$  nanorods on its surface was formed. To check the proposed mechanism, we have done several parallel experiments with shorter reaction time of 10 and 6 h with the other synthetic conditions remaining unchanged. It was found that with the decrease of the reaction time, there were more separated nanorods in the products. This result is consistent with the formation mechanism of the  $\text{Sb}_{2-x}\text{Bi}_x\text{S}_3$  flowers.

Optical absorption experiments were carried out to elucidate the band gap energy, which is one of the most important electronic parameters for semiconductor nanomaterials. Figure 5 shows typical UV–Vis absorption spectra of the two samples. The  $\lambda_{\text{onset}}$  of the spectra recorded from the two samples are about 940 and 955 nm for  $x = 0.4$  and 1.0, respectively. The band gap of the  $\text{Sb}_{2-x}\text{Bi}_x\text{S}_3$  may be estimated using the following formula:

$$(\alpha hv)^2 = B(hv - E_g) \quad (1)$$

where,  $\alpha$  is the absorption coefficient,  $hv$  is the photon energy,  $B$  is a constant characteristic of the material, and  $E_g$  is the band gap. The value of  $hv$  extrapolated to  $\alpha = 0$  gives the absorption band gap energy. The band gaps of the  $\text{Sb}_{2-x}\text{Bi}_x\text{S}_3$  are calculated to be 1.32 and 1.30 eV for  $x = 0.4$  and 1.0, respectively, which are smaller than the values reported for pure  $\text{Sb}_2\text{S}_3$ , but are near to that of  $\text{Bi}_2\text{S}_3$ . The change in band gap energy probably result from the change in the composition of the  $\text{Sb}_{2-x}\text{Bi}_x\text{S}_3$ , since

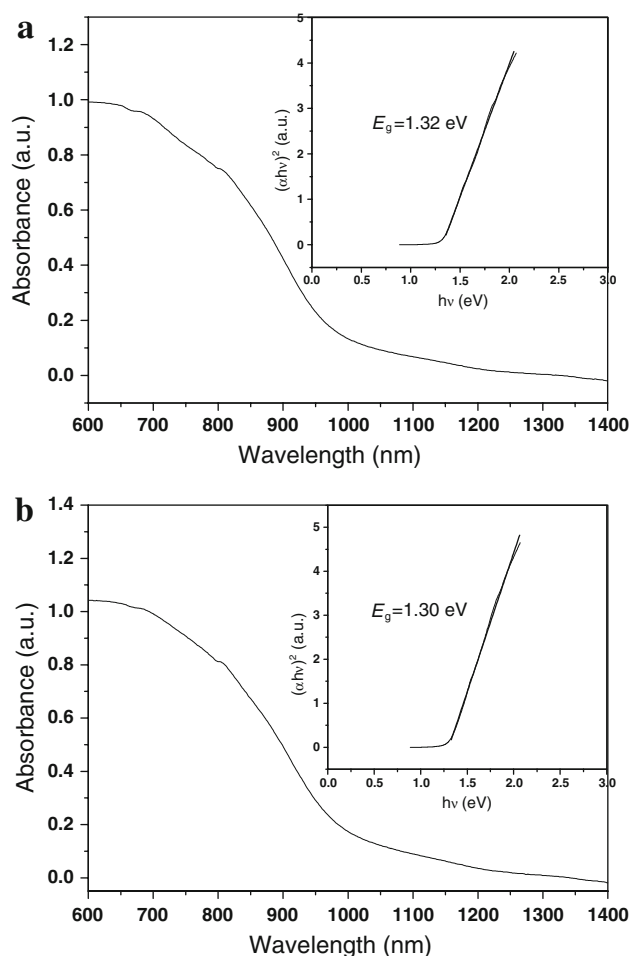


**Fig. 5** UV–Vis spectra of the  $\text{Sb}_{2-x}\text{Bi}_x\text{S}_3$ : **a**  $x = 0.4$ ; **b**  $x = 1$ . The insets contain the corresponding  $(\alpha hv)^2$  versus  $hv$  curves

the flower-like  $\text{Sb}_{2-x}\text{Bi}_x\text{S}_3$  nanostructures in our dimensional range should not show a quantum confinement effect due to the low Bohr radius of these materials. The flower-like  $\text{Sb}_{2-x}\text{Bi}_x\text{S}_3$  nanostructures with a narrow band gap may be very promising for applications in solar energy and photoelectronics.

## Conclusions

In summary, we have developed a facile and mild solvothermal method for the large-scale preparation of ternary sulfide  $\text{Sb}_{2-x}\text{Bi}_x\text{S}_3$  ( $x = 0.4, 1.0$ ) flower-like nanostructures. The possible formation mechanism of the flower-like  $\text{Sb}_{2-x}\text{Bi}_x\text{S}_3$  is suggested. The optical properties of the  $\text{Sb}_{2-x}\text{Bi}_x\text{S}_3$  products were evaluated by UV–Vis spectroscopy at ambient temperature. The results indicate that the  $\text{Sb}_{2-x}\text{Bi}_x\text{S}_3$  compounds are semiconducting with direct band gaps of 1.32 and 1.30 eV for  $x = 0.4$  and 1.0, respectively. This method can probably be extended to the

fabrication of other ternary sulfide semiconductors nanostructures with various morphologies and functions.

**Acknowledgments** We are grateful for financial support from the Natural Science Foundation of Jiangsu Province (No. BK2009196) and the National Natural Science Foundation of China (No. 20875039).

## References

1. K.J. Tang, J.N. Zhang, W.F. Yan, Z.H. Li, Y.D. Wang, W.M. Yang, Z.K. Xie, T.L. Sun, H. Fuchs, *J. Amer. Chem. Soc.* **130**, 2676 (2008)
2. Y. Liu, Q. Shen, D. Yu, W. Shi, J. Li, J. Zhou, X. Liu, *Nanotechnology* **19**, 245601 (2008)
3. J. Black, E.M. Conwell, L. Seigle, C.W. Spencer, *J. Phys. Chem. Solids* **2**, 240 (1957)
4. B.X. Chen, C. Uher, L. Iordanidis, M.G. Kanatzidis, *Chem. Mater.* **9**, 1655 (1997)
5. R.S. Mane, B.R. Sankapal, C.D. Lokhande, *Mater. Chem. Phys.* **60**, 196 (1999)
6. Y. Yu, R.H. Wang, Q. Chen, L.M. Peng, *J. Phys. Chem. B* **109**, 23312 (2005)
7. B. Roy, B.R. Chakraborty, R. Bhattacharya, A.K. Dutta, *Solid State Commun.* **25**, 937 (1978)
8. O. Savadogo, K.C. Manda, *Solar Cells* **26**, 117 (1992)
9. M.T.S. Nair, Y. Pena, J. Campos, V.M. Garica, P.K. Nair, *J. Electrochem. Soc.* **141**, 2113 (1998)
10. J. Geroge, M.K. Radhakrishnan, *Solid State Commun.* **33**, 987 (1980)
11. O. Savadogo, K.C. Mandal, *Electron. Lett.* **28**, 1682 (1992)
12. A.M. Salem, M.S. Selim, *J. Phys. D Appl. Phys.* **34**, 12 (2001)
13. K.Y. Rajpure, C.D. Lokhande, C.H. Bhosale, *Mater. Res. Bull.* **34**, 1079 (1999)
14. Y.L. Soo, Z.H. Ming, S.W. Huang, Y.H. Kao, *Phys. Rev. B* **50**, 7602 (1994)
15. D. Son, D.R. Jung, J. Kim, T. Moon, C.J. Kim, B. Park, *Appl. Phys. Lett.* **90**, 101910 (2007)
16. J.P. Ge, J. Wang, H.X. Zhang, X. Wang, Q. Peng, Y.D. Li, *Adv. Funct. Mater.* **15**, 303 (2005)
17. W.Z. Wang, I. Germanenko, *Chem. Mater.* **149**, 3028 (2004)
18. D.V. Petrov, B.S. Santos, G.A.L. Pereira, C. de Mello Donegá, *J. Phys. Chem. B* **106**, 5325 (2002)
19. X.P. Shen, H. Zhao, Q. Liu, Z. Xu, *Chin. J. Inorg. Chem.* **23**, 1561 (2007)
20. X.P. Shen, G. Yin, W.L. Zhang, Z. Xu, *Solid State Commun.* **140**, 116 (2006)